Astron. Astrophys. 164, 208–217 (1986)

ASTRONOMY AND ASTROPHYSICS

The structure and dynamics of evolved supernova remnants. Shock-heated dust in the Cygnus Loop

R. Braun[1] **and R. G. Strom**[2]

[1] Sterrewacht Leiden, Postbus 9513, 2300 RA Leiden, The Netherlands
[2] Netherlands Foundation for Radio Astronomy, Postbus 2, 7990 AA Dwingeloo, The Netherlands

Received January 2, accepted March 15, 1986

Summary. Observations of shock-heated dust in the Cygnus Loop made with IRAS at 12, 25, 60, and 100 µm are presented and analyzed. A bright shell is observed, coincident with the optical nebulosity and X-ray emission. Beam reconstruction and background removal techniques are employed to map the pre-shock density distribution within the shell. Emission characteristics are well described by current models of shock-heated dust if account is taken of the effects of an incomplete cooling layer and the presence of recombined gas. A revised distance estimate ($D=460\pm 160$ pc) is obtained and the environment of the SNR are discussed.

The evidence presented here as well as other recent observations very strongly suggest the existence of a high density shell which pre-dates the SNR. Optical observations of radially structured ionization zones and the apparent energy-diameter relationship for SNR suggest that this is a general phenomenon.

Key words: Supernova remnants – Cygnus Loop – dust – bubbles

1. Introduction

The Cygnus Loop as one of the nearest evolved supernova remnants (SNR) at high galactic latitude provides an opportunity to study a variety of shock-related phenomena with almost unequaled sensitivity and linear resolution against a relatively unconfused background. These favorable circumstances have led to the acquisition of constraints which increasingly limit the set of acceptable theories in regard to its evolutionary state, as well as SNR evolution in general. A relatively new tool in the study of SNR has been the observation of shock-heated dust emission in the infrared. The prodigious emission from collisionally heated dust in the ISM has proved a valuable diagnostic (eg. Braun, 1986) when used in combination with other constraints.

Here we will add to the body of observational constraints for the Cygnus Loop with images at 12, 25, 60, and 100 µm made with the Infrared Astronomical Satellite (IRAS). The observations and data reduction procedures are discussed in Sect. 2, including the special considerations necessary for evolved SNR where a significant fraction of the shocked gas has (locally) recombined. In Sect. 3.1 we consider the available evidence concerning the environment of the SNR and arrive at an improved distance estimate. The implications of the observed brightness distribution found in the present as well as in previous studies are considered in Sect. 3.2; while Sect. 3.3 deals with the physical parameters we derive. Conclusions are summarized in Sect. 4.

Send offprint requests to: R. Braun

* Now at National Radio Astronomy Observatory, PO Box 0, Socorro, NM 87801, USA

2. Observations and data reduction

2.1. Gaussian beam recovery and background removal

The Cygnus Loop was observed with the IRAS survey instrument detector array (IRAS, 1985) at 12, 25, 60, and 100 µm as part of the satellite's all-sky survey. The calibrated detector data (CRDD) from the first two independent sky coverages (HCON 1 and HCON 2) was gridded using standard software. Since the calibration history of this data is still poorly documented, the relative calibration with respect to the IRAS Skyflux (HCON 3) final product was determined by plotting the corresponding brightnesses at a similar resolution from identical grids covering a smoothly varying test field. The well-defined linear relationship has slope (CRDD/Skyflux) (1.3 ± 0.1; 1.6 ± 0.3; 1.4 ± 0.1; 1.4 ± 0.1) in the 12, 25, 60, and 100 µm bands respectively. This is consistent with a constant linear scaling with factor 0.71 ± 0.05 to obtain Skyflux surface brightnesses from CRDD data in each band. This factor has been applied to the data for the sake of consistency with the IRAS final products. The response to a bright unresolved source at $\alpha=20^h53^m$, $\delta=30°15'$ was masked out of the 12 and 25 µm images to prevent degradation of a larger map area during subsequent processing. The intrinsic instrumental response is both different in each of the four wavelength bands and awkward in the sense of having a relatively flat top and steep sides. In order to obtain identical Gaussian beams in each band the procedure discussed by Braun (1986) was adopted. The images were processed by applying a linear deconvolution using an analytic model of the point source response, followed by a Gaussian spatial frequency taper truncated at the 1% level. Each image was transformed in this way to the limiting Gaussian resolution of the 100 µm band survey detectors: 6.′9 × 4.′6. The two independent data sets were then combined to yield the maps shown in Fig. 1. Large-scale hysteresis effects for the detector array (IRAS, 1985) should not be present in the data since the scan path (from south-

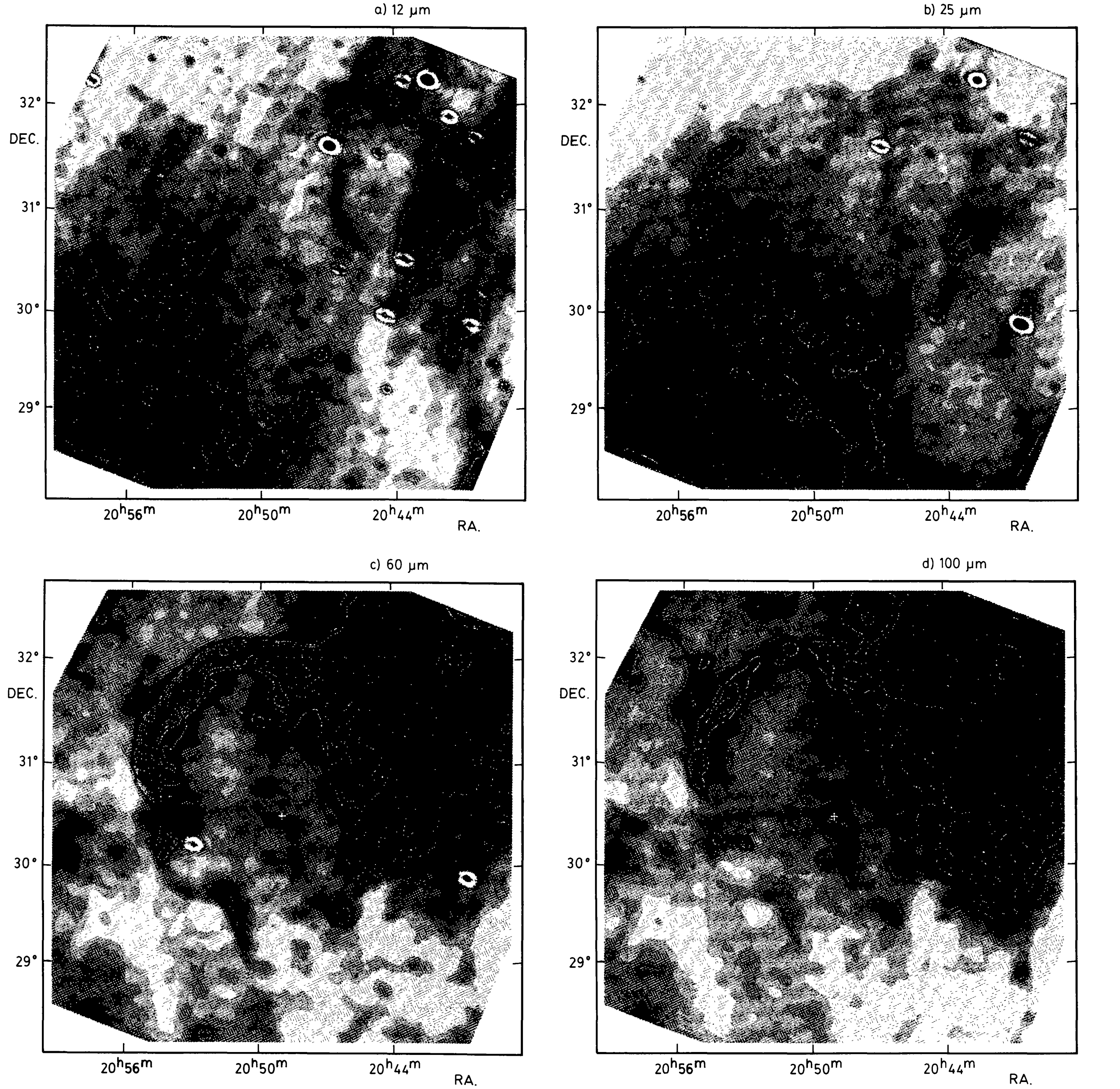

Fig. 1a–d. Dust emission from the Cygnus Loop and environment as observed in the 12, 25, 60, and 100 μm bands of IRAS. The beam in all four bands is an elliptical Gaussian (6'.9 × 4'.6 at position angle $\phi = 66^\circ.5$). The grey scale in each map is based on a histogram of map intensities. Contours are in units of nominal surface brightness. The contour levels increase logarithmically by a factor 1.2 from the lowest value. **a** 12 μm image. The lowest contour level is 0.60 MJy/sr. **b** 25 μm image. The lowest contour level is 0.92 MJy/sr. **c** 60 μm image. The lowest contour level is 1.78 MJy/sr. **d** 100 μm image. The lowest contour level is 7.1 MJy/sr

east to north-west) has not yet crossed any region of intense emission. The effect of localized hysteresis is apparent in the "comet tails" which extend to the north-west of the brightest stars. The emission from the Cygnus Loop itself is not bright enough to result in significant hysteresis at any wavelength. The effect of truncating the spatial frequency taper is also visible near the brightest stars as faint (0.3 %) concentric sidelobes.

While the Cygnus Loop emission can be readily distinguished in the raw maps, (most obviously at 60 μm) it is clear that the background confusion from zodiacal light (in the south-east) and cool dust (in the north-west) limits the utility of the data. Since the spectra of each of these components is distinct, a two-dimensional spectral decomposition utilizing the four observed bands should allow their separation (as discussed by Braun, 1986). Initial estimates of the component spectra were iteratively adjusted so as to obtain featureless residuals and strictly positive component maps with a minimum degree of correlation with one another. Map areas containing bright stars, background galaxies or H II regions were not represented by the three component spectra and could therefore not be simultaneously fit. Such (isolated) map areas will

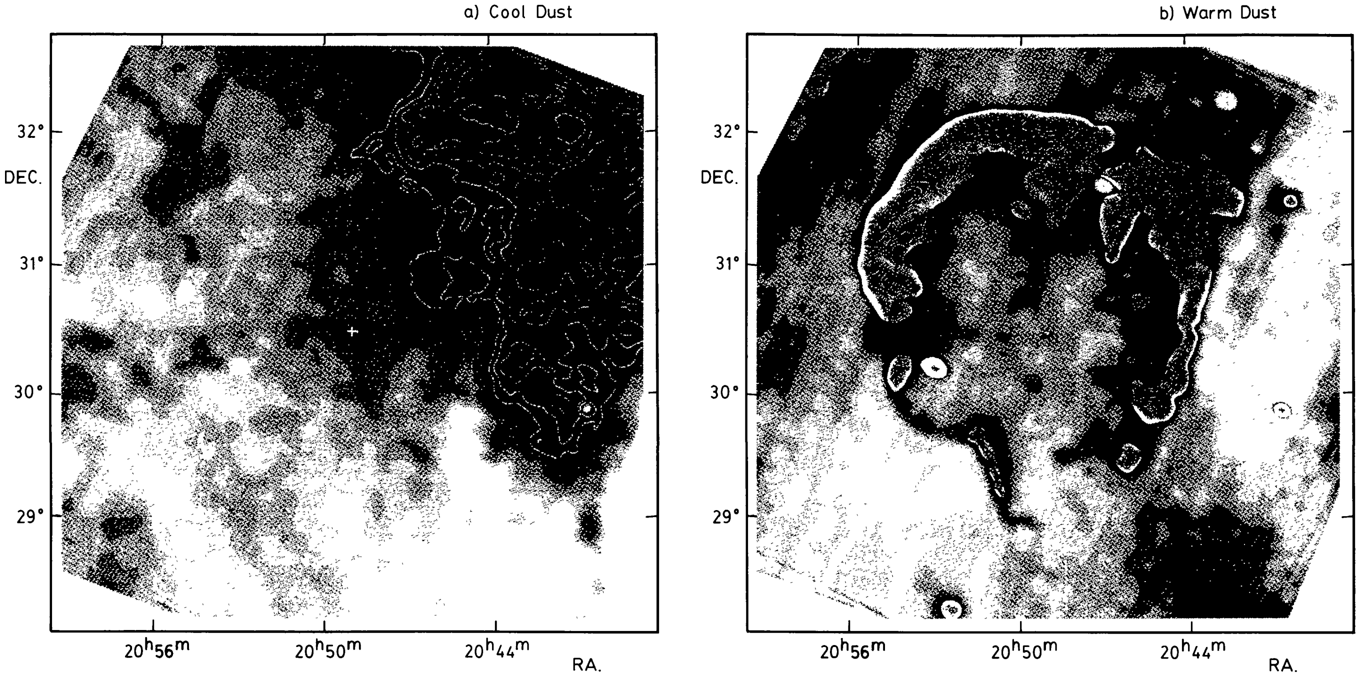

Fig. 2a and b. Cool and warm dust emission components derived from the maps in Fig. 1 by a three component spectral decomposition. The grey scale is based on a histogram of map intensities. Contours are in units of nominal surface brightness in the 100 μm band. The contour levels increase logarithmically by a factor 1.2 from the lowest value. **a** Cool dust component. The lowest contour level is 12.0 MJy/sr. **b** Warm dust component. The lowest contour level is 0.63 MJy/sr

not be considered in the subsequent analysis. The SNR (nominal brightness ratios at 12:25:60:100 μm = 0.046:0.074:0.600:1.000) and cool dust (nominal brightness ratios = 0.023:0.027:0.178:1.000) component maps so derived are shown in Fig. 2. These components have been quite effectively isolated, although the diminished baseline quality near the map edges (a property of the standard grid addition program) is reflected in the less satisfactory fit in these areas. The four maps of Fig. 1 were subsequently corrected for the background by subtracting the appropriately scaled versions of the cool dust component (Fig. 2a) and a quadratic surface fit to the zodiacal light component (not shown but with nominal brightness ratios = 0.49:1.00:0.45:0.18) from each. In this way, any real spectral variations across the source, which lead to small scale structure in the zodiacal light component and the fit residuals, are not removed from the data. The resulting images are shown in Fig. 3.

2.2. *Spectral parameters*

The emission expected from shock-heated dust within SNR has been discussed by Draine (1981) and Braun (1986). Collisional heating of dust grains in a high temperature gas ($T > 10^5$ K) gives rise to prodigious infrared emission while the grains are being sputtered. The energetic shocks of young SNR tend to destroy the entire grain population before the gas cools, while the more rapid cooling within high density clouds engulfed by an evolved SNR allows recombination of the gas, leaving a partially intact grain population. The dust within the recombined gas will be heated by the local radiation field and radiate according to the usual energy balance condition. Dust which has undergone shock processing will have been modified in the following ways: 1. the entire grain population will have suffered a decrease in grain radius due to sputtering which is approximately linear with time and 2. the entire small particle end of the size distribution ($a < 10^{-7}$ cm) will have been destroyed on a short time scale due to thermal sublimation and catastrophic disruption (cf. Draine, 1981). The emission spectrum of such processed dust should be more adequately described by a single temperature model, in contrast to the 12 and 25 μm excesses caused by an extensive small particle population which is subject to single photon heating (cf. Draine and Anderson, 1985). In fact, the temperature of the large particles occurring immediately outside of the SNR and of those within the recombined gas should be similar, given the similar radiation field to which both are exposed.

Before analysis of the shock-heated dust component within an evolved SNR, it must be effectively isolated from the cool, recombined component with which it will be in close proximity. The spectral decomposition discussed above may partially filter the recombined gas from the background corrected images in areas where the recombined and collisionally heated gas are not well mixed. However, the uniformity of the cool dust distribution (Fig. 2a) suggests that this has not been a very significant effect. (One notable exception is the loop-like filament at $\alpha = 20^h54^m$, $\delta = 30°30'$ which appears (morphologically) to be SNR related yet is almost fully absorbed into the cool dust component. This feature has no obvious X-ray, optical or radio counterpart, yet should perhaps be visible in recombined H I (cf. Braun and Strom, 1986) if it is SNR related). We will assume that the majority of recombined gas has been retained in the background corrected images.

Integrated nominal fluxes were derived from the maps in Fig. 3 after masking out all stellar and warm compact sources. These fluxes (listed in Table 1) were compared to simulated nominal fluxes derived from frequency band integrations of a model spectrum. This model was based on a single temperature silicate and graphite grain population (using the absorption efficiencies derived by Draine and Lee, 1984 and tabulated by Draine, 1985). In contrast to young SNR (Tycho, Kepler, Cas A and G292.0

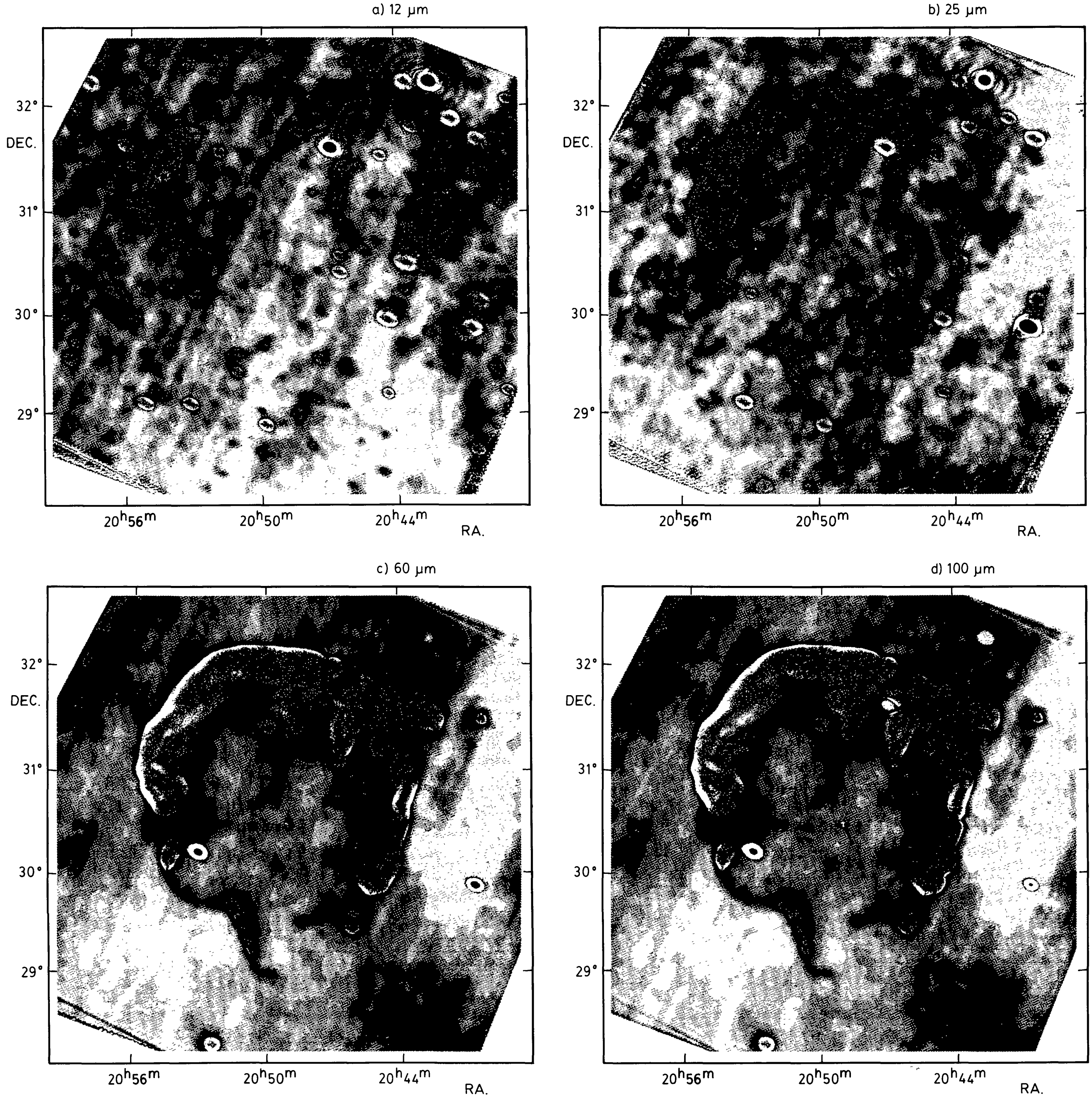

Fig. 3a–d. Background corrected warm dust emission from the Cygnus Loop in the IRAS 12, 25, 60, and 100 μm bands. The maps are those of Fig. 1 after subtraction of the scaled cool dust component (Fig. 2a) and a second order surface fit to the zodiacal light component. The grey scale is based on a histogram of map intensities. Contours are in units of nominal surface brightness. The contour levels increase logarithmically by a fixed factor from the lowest contour level. **a** 12 μm image. The factor is 1.3 and the lowest contour 0.24 MJy/sr. **b** 25 μm image. The factor is 1.3 and the lowest contour 0.227 MJy/sr. **c** 60 μm image. The factor is 1.1 and the lowest contour 1.20 MJy/sr. **d** 100 μm image. The factor is 1.1 and the lowest contour 2.00 MJy/sr

+1.8; Braun, 1986; Braun et al., 1986) and in accordance with the discussion above, the 25, 60, and 100 μm fluxes of the Cygnus Loop could not be fit by a single temperature model. The striking abuttment of the SNR and cool dust components along the north-west boundary (Fig. 2a and b) suggests that these components are physically associated. The spectrum of the external dust (nominal brightness ratios at 12:25:60:100 μm =0.023:0.027:0.178:1.000), stripped of its small particle content (nominal brightness ratios =0.000:0.000:0.178:1.000), should then be appropriate for the recombined gas within the SNR. A unique single temperature average spectrum (nominal brightness ratios = – :0.16:1.00:0.47) is then implied by the integrated fluxes and the spectrum of the recombined gas component. The corresponding nominal fluxes for both the shock-heated and

Table 1. Infrared spectral parameters

		Total	Shock-heated	Recombined
Nominal flux density	(12 μm)	(38.)	(38.)	(0.)
[Jy]	(25 μm)	172. ± 17.	172. ± 17.	(0.)
	(60 μm)	1430 ± 140	1070 ± 110	355. ± 35.
	(100 μm)	2490 ± 250	505. ± 50.	1980 ± 200
Color corrected flux	(12 μm)		(38.)	(0.)
[Jy]	(25 μm)		207. ± 30.	(0.)
	(60 μm)		1050 ± 160	295. ± 45.
	(100 μm)		465. ± 70.	2070 ± 310
Color corrected λI_λ	(12 μm)		(4.35 10^{-9})	(0.)
[$\mathrm{W\,m^{-2}\,sr^{-1}}$]	(25 μm)		1.15 ± 0.17 10^{-8}	(0.)
	(60 μm)		2.45 ± 0.37 10^{-8}	6.9 ± 1.0 10^{-9}
	(100 μm)		6.5 ± 1.0 10^{-9}	2.90 ± 0.44 10^{-8}
λ_{peak} [μm]			43.5 ± 0.5	
$\lambda I_\lambda^{\mathrm{max}}$ [$\mathrm{W\,m^{-2}\,sr^{-1}}$]			3.35 ± 0.50 10^{-8}	
Angular radius [degrees]			1.5	1.5

(.) Uncertain values

recombined components are listed in Table 1. Color corrections (to compensate for the detector bandwidth) and the peak wavelength, λ_{peak} and surface brightness, $\lambda I_\lambda^{\mathrm{max}}$ were derived from the single temperature models and are also listed in Table 1.

3. Discussion

3.1. Distance and environment

The widely accepted estimate of the distance to the Cygnus Loop ($D = 770$ pc) is due to Minkowski (1958). In his Fig. 1 are plotted the radial velocities $\pm 10\,\mathrm{km\,s^{-1}}$) of 37 diffuse and filamentary features against their distance from the center of the SNR. While there is considerable intrinsic spread in the data with regard to the narrow velocity ellipse expected from a constant velocity spheroid, there is also a clear indication of systematic expansion. In fact, the diffuse and filamentary features taken separately appear to define two distinct ellipsoids; the diffuse extending to higher velocity and smaller radius and the filamentary to lower velocity and larger radius. This pattern is suggestive of the evaporating ram-pressure accelerated cloud scenario of McKee et al. (1978). Unfortunately, the relatively small number of existing data points does not permit separate treatment of these systems with sufficient statistical significance. It is also noteworthy that all measured radial velocities are either near $V_{\mathrm{lsr}} = 0\,\mathrm{km\,s^{-1}}$ or negative, suggesting that most optical filaments and therefore high density ambient clouds are in the plane of the sky or on the approaching face of the SNR. The concentration of features at large radius near $V_{\mathrm{lsr}} = 15 \pm 5\,\mathrm{km\,s^{-1}}$ led Minkowski to adopt this as the systematic velocity. There are other indications which also favor this value. The neutral hydrogen distribution (DeNoyer, 1975) in the velocity interval $V_{\mathrm{lsr}} = 0$ to $10\,\mathrm{km\,s^{-1}}$ delineates a cloud complex to the west and north of the SNR which is also apparent in the diminished star density on the POSS E plate. This complex contains CO clouds (Scoville et al., 1977) with $V_{\mathrm{lsr}} = +11\,\mathrm{km\,s^{-1}}$ which appear to about the bright optical filaments in the west. The complex is perhaps best seen in the cool dust component of the infrared emission shown in Fig. 2a. The cool dust emission is very well correlated with the neutral hydrogen, showing the same bright ridge in the west and north, gradual decline to the east and south, and the local peak just beyond the northeastern optical filaments. Local peaks are also coincident with CO clouds in the west. The northwestern boundary of the SNR is strikingly delineated by the cool dust distribution, including an almost rectangular corner which has apparently already undergone shock passage (cf. Fig. 2b). This point will be discussed further below. Since both the declining shelf region to the east of the bright western ridge and the bright north-western hook appear in the H I distribution at velocities between $V_{\mathrm{lsr}} = 0$ and $+10\,\mathrm{km\,s^{-1}}$, it seems likely that these features are between us and the Cygnus Loop (for which $V_{\mathrm{sys}} \sim +15\,\mathrm{km\,s^{-1}}$) and that they form the high density region which has led to the negative velocity (front-face) optical filaments.

Having established a probable systemic velocity, the radial velocity data can be used to determine the best-fitting position-velocity ellipsoid. Writing the space velocity as the sum of perpendicular components, $v^2 = v_r^2 + v_t^2$ and substituting $v_t = D\theta\,(v_\theta/\theta)$, gives $v_r^2 = v^2 - D^2\,(v_\theta/\theta)^2\,\theta^2$, so that a plot of v_r^2 vs θ^2 yields a slope $-D^2\,(v_\theta/\theta)^2$ and intercept v^2. The linear regression solution for the 37 available points yields an expansion velocity $v = 65 \pm 23\,\mathrm{km\,s^{-1}}$ (one standard deviation error). Equating the expansion velocity with the proper motion observed by Hubble (1937) for the brightest optical filaments (NGC 6960 and NGC 6992) of $0''.03\,\mathrm{yr^{-1}}$ allows the derivation of the distance $D = 460 \pm 160$ pc assuming similar average densities in the front face and sky plane ambient clouds. (It will be shown below that these densities are indeed similar.)

3.2. Brightness distribution

The Cygnus Loop as the archetypal middle aged SNR has been studied in all available wavelength bands. Its proximity provides for low absorption and very high linear resolution.

The brightest X-ray emission is concentrated in an almost circular (84 ± 5′), limb-brightened filamentary shell (best seen in the Einstein IPC composite of Ku et al., 1984), with an extension

($\sim 30'$) to the south. The X-ray spectrum of the bright shell is reasonably well fit be a single temperature thermal plasma with $T \sim 2\ 10^6$ K corresponding to a shock velocity $v_s \sim 360\ \mathrm{km\,s^{-1}}$ (Ku et al., 1984; Charles et al., 1985). This emission is superposed on a faint plateau extending 20′ to 30′ further to the west and south and $\sim 10'$ elsewhere. (This plateau is distinct from the brighter ridges at smaller radii which correspond to the optical Balmer line filaments.) According to Ku et al. (1984) the reality of the faint emission plateau is beyond doubt. The implication is clear. The intercloud shock, propagating in a low density, high filling factor medium is significantly outside of the bright filamentary shell. This is perhaps not too surprising since the fact that the brightest emission has a great deal of small-scale structure already suggests that it is associated with a component of relatively small filling factor. The current location of the outer shock cannot be accurately determined, but it must lie at least as far beyond the bright filaments as the plateau emission. A diffuse high temperature shell extending to a radius 20–30% greater than the bright shell seems indicated. The contribution of such a thick shell would influence the X-ray spectrum in regions of fainter emission on the front face of the SNR. Spectra at such positions do require higher temperatures, $T > 4\ 10^6$ and are indicative of a second harder component of emission (Ku et al., 1984; Charles et al., 1985). This has been interpreted as evidence for a hot interior, although in light of the present discussion a hot exterior may also be a contributing factor. The bright filamentary shell on the other hand is well correlated with optical and radio emitting filaments which almost certainly represent recombining high density clouds engulfed by the blast wave. Enhanced X-ray emission might be expected from either intrinsically lower density ($n_\mathrm{H} < 1\ \mathrm{cm^{-3}}$) portions of such clouds or their evaporating edges (Cowie and McKee, 1977).

The optical emission from the Cygnus Loop is associated with a wide variety of filament types. The various degrees of ionization within the brightest filamentary systems in the northeast, north-center and west are seen in the narrow-band interference filter photographs of Fesen et al. (1982). There is a clear tendency for the diffuse, lower ionization filaments (showing bright [O I] followed by [S II], H_α^+ [N II] to be at smaller radii than the crisper, high ionization filaments, brightest in [O III]. If a complete cooling layer is present, i.e. the encountered clouds have thicknesses $\geqq 0.002$ pc, then the [O III] line intensity should increase monotonically with shock velocity in the range $v_s = 50$ to $140\ \mathrm{km\,s^{-1}}$ (e.g. Raymond, 1979) for a fixed ambient density. Fesen et al. (1982) consider the possibility that most clouds are so thin that a full cooling layer does not exist. However, explanation of the large systematic radial displacement of the filament types then makes unreasonable demands on the geometry. Since such displacements are a natural consequence of shock propagation in relatively thick clouds, this seems the more likely alternative. At least two possible interpretations present themselves within this context. The clouds are so thick that the long shock passage times have allowed the inter-cloud shock to progress far enough that the pressure driving the cloud shock has significantly decreased. However, if the intercloud shock is approximately adiabatic (as is likely) the pressure decrease over the width of the entire filament complex ($<10'$, or $<10\%$ of the radius) is only $\sim 40\%$ (cf. Chevalier, 1974), so that only $a \sim 20\%$ variation in velocity could be expected for a population of clouds with similar average densities. The other obvious possibility (mentioned by Fesen et al., 1982, but not considered further) is that there is a real decrease in the mean cloud density with radius. This point will be discussed at more length below.

Spectra of the bright filaments have been fit with varying success by steady-flow shock models with velocities $v_s = 70$ to $130\ \mathrm{km\,s^{-1}}$ and pre-shock densities, $n_0 \sim 10\ \mathrm{cm^{-3}}$. In particular, Raymond (1979) suggests that depleted carbon and silicon, a shock velocity $v_s = 70\ \mathrm{km\,s^{-1}}$ and a density $n_0 = 10$ to $20\ \mathrm{cm^{-3}}$ provide a reasonable fit to Miller's (1974) position 1 and 2 (within the bright northeastern filamentary system). Such a velocity is in good agreement with the expansion rate found above.

A faint system of predominantly Balmer line filaments has also been recognized (e.g. Raymond et al., 1980) which is typically found to have a 5 to 10′ larger radius than the nearest "normal" emission line filaments. These filaments have been interpreted as arising in a non-radiative shock within partially neutral ambient gas, analogous to those seen in Tycho (e.g. Chevalier and Raymond, 1978). The current estimates of shock parameters (Raymond et al., 1983) are velocity $v_s = 200\ \mathrm{km\,s^{-1}}$ and pre-shock density $n_0 > 3\ \mathrm{cm^{-3}}$ (at the distance $D = 460$ pc). As noted above, these filaments appear to have bright X-ray counterparts suggesting that even lower density gas must be associated with them.

Many of the optical and X-ray filaments are also seen in the radio brightness distribution (Keen et al., 1973; Dickel and Willis, 1980; Green, 1984) although there is great variation in the relative brightness seen in the three bands. This suggests a similarly large range of local conditions. A general increase in diffuse radio brightness is seen to the south and west, while the narrow radio filaments have similar brightness at most locations. There is also an indication of localized diffuse emission extending 20′ to 30′ beyond the bright western rim and the southern extension (features W and E mapped by Green, 1984) where the X-ray plateau is also most prominent. This provides further evidence that the inter-cloud shock is significantly beyond the "normal" and Balmer emission line filaments delineated by the bright X-ray shell.

The background corrected IR images at 12, 25, 60, and 100 μm are shown in Fig. 3. The overall structure, and its striking similarity to the optical and X-ray images is especially clear at 60 and 100 μm while only the brighter filaments remain visible in the 12 and 25 μm bands. Some residual background structure in the form of diffuse low brightness peaks and depressions is evident along the edges of the field. The unresolved stellar images most prominent at 12 and 25 μm give a good indication of the beam size ($6\rlap{.}'9 \times 4\rlap{.}'6$ FWHM elliptical Gaussian elongated in position angle $\phi = 66\rlap{.}^\circ5$). The brightest dust emission is associated with the major optical filament complexes and the faint Balmer line arc enclosing the entire northern quadrant as illustrated in Fig. 4. The south-eastern X-ray limb is also well-defined. The magnitude of residual background variations does not allow a deep search for a counterpart to the faint X-ray plateau, although a very clear IR extension is seen to the north-west $\sim 15'$ beyond the bright X-ray/IR rim. However, the unresolved peak at $\alpha = 20^\mathrm{h}42^\mathrm{m}24^\mathrm{s}$, $\delta = 31°30'49''$ is coincident with the B3 star AGK3 +31 2076, and is most likely unrelated. The two bright peaks in the northwest (at $\alpha = 20^\mathrm{h}42^\mathrm{m}$, $\delta = 32°10'$ and $\alpha = 20^\mathrm{h}47^\mathrm{m}$, $\delta = 31°40'$) which are prominent at 60 and 100 μm, appear to be unrelated stars. Two other compact peaks seen at 60 and 100 μm in the west and east-center (at $\alpha = 20^\mathrm{h}41^\mathrm{m}$, $\delta = 29°52'$ and $20^\mathrm{h}53^\mathrm{m}$, $\delta = 30°10'$) are unidentified, presumably background objects. The striking coincidence of a prominent depression in the northern rim at $\alpha = 20^\mathrm{h}48^\mathrm{m}$, $\delta = 32°$ with cool dust and H I emission is suggestive of a physical association (since absorption at wavelengths > 50 μm would imply H I column densities $N_\mathrm{H} > 10^{24}\ \mathrm{cm^{-2}}$). The widespread dust emission and its correlation with optical filaments suggests that depleted carbon and silicate abundance should be expected in the

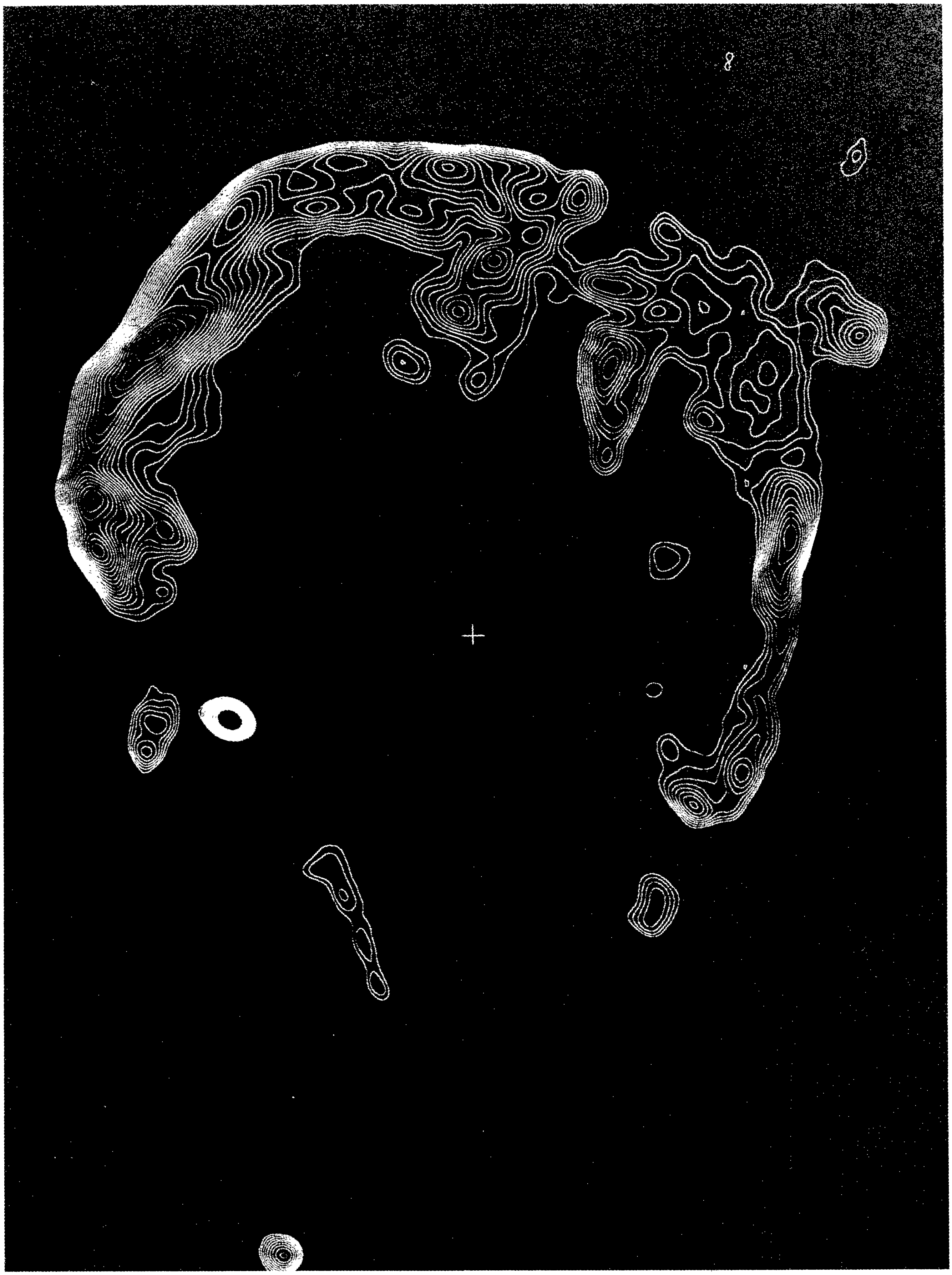

Fig. 4. Warm dust and recombining gas. Contours of the 60 µm background corrected warm dust emission (Fig. 3c) overlaid on the POSS E plate

optical spectra as was inferred by Raymond (1979) and Raymond et al. (1980).

3.3. Physical parameters

The infrared spectral data for the integral properties of the shock-heated dust emission correspond to a spectral peak at $\lambda_{peak} = 43.5 \pm 1\ \mu m$ and peak surface brightness, $\lambda I_\lambda^{max} = 3.35\ 10^{-8}\ W\,m^{-2}\,sr^{-1}$, assuming a shock radius $\theta_s = 1\overset{\circ}{.}5$. Relationships between these and the physical parameters: local shock velocity, v_c, local density, n_c, and volume filling factor of the dominant high density component, f_c, are given by Braun (1986) based on the model calculations of Draine (1981). The appropriate expressions are

$$\lambda I_\lambda^{max} \simeq 6.96\ 10^{-6} f_c \left[16 \left(\frac{n_c \tau}{5\ 10^4}\right)^{1/2} - 15 \left(\frac{n_c \tau}{5\ 10^4}\right)\right] \cdot \left(\frac{n_c}{cm^{-3}}\right)\left(\frac{v_c}{10^3\ km\,s^{-1}}\right)^3 W\,m^{-2}\,sr^{-1} \quad (1a)$$

for $n_c \tau < 5\ 10^3\ cm^{-3}\ yr$ and $v_c \lesssim 1200\ km\,s^{-1}$

$$\lambda I_\lambda^{max} \simeq 3.48\ 10^{-5} f_c \left(\frac{n_c}{cm^{-3}}\right)\left(\frac{v_c}{10\ km\,s^{-1}}\right)^3 W\,m^{-2}\,sr^{-1} \quad (1b)$$

for $n_c \tau > 10^4\ cm^{-3}\ yr$

and

$$\lambda_{peak} \simeq 37.6 \left(\frac{n_c}{cm^{-3}}\right)^{-0.18} \left(\frac{v_c}{10^3\ km\,s^{-1}}\right)^{-0.3} \mu m \quad (2)$$

(Eqs. (3), (4) and (5) from Braun, 1986) in which τ is the average time since shock encounter for the region of emission.

The brightest shock-heated dust emission is associated with the bright optical filaments which have high densities and low shock velocities, $v_s \sim 65\ km\,s^{-1}$ (based on the average expansion velocity above and the model comparisons of Raymond, 1979). Somewhat less intense IR emission is associated with the faint Balmer line/X-ray filaments, for which lower densities and higher shock velocities, $v_s \sim 200\ km\,s^{-1}$ apply (Raymond et al., 1983). The faintest discernible emission is associated with the remaining portions of the bright X-ray shell. A representative shock velocity for the IR emitting gas is thus $v_c \sim 130\ km\,s^{-1}$ which corresponds to a pre-shock density $n_c = 13\ cm^{-3}$ via Eq. (2). With a given shock ram pressure (fixed nv^2) Eq. (1a) predicts a surface brightness $\lambda I_\lambda \sim$ const., while Eq. (1b) predicts $\lambda I_\lambda \propto n^{-1/2}$. The trend observed above is more consistent with the low $n_c \tau$ regime described by Eq. (1a). With the shock velocity and density derived above, the value of τ will be determined by the recombination time in a depleted gas, $\tau \simeq 300$ yr (Raymond, 1979) when collisional heating of the gas ceases. The volume filling factor given by Eq. (1a) for the dust emitting gas, $f_c \simeq 0.05$ is consistent with a clumpy shell. Since the X-ray spectrum of the bright shell is well fit by a single temperature thermal plasma, corresponding to a shock velocity, $v_s = 360\ km\,s^{-1}$, the pre-shock density of the material (assuming pressure equilibrium) is $n_s = 1.7\ cm^{-3}$.

Another effect which should be observable is the spectral variation caused by variations in the pre-shock density. At a fixed ram pressure, Eq. (2) predicts, $\lambda_{peak} \propto n_c^{-0.03}$ so that the spectrum should shift to shorter wavelengths for higher ambient densities. This is graphically illustrated by the 60/100 µm ratio map in Fig. 5. Optical forbidden line filaments can be clearly identified by their "warmer" color, corresponding to higher pre-shock densities, while the Balmer line/X-ray filaments have systematically "cooler" colors and lower implied densities. (Unresolved peaks which appear in this distribution are residual star images and should be

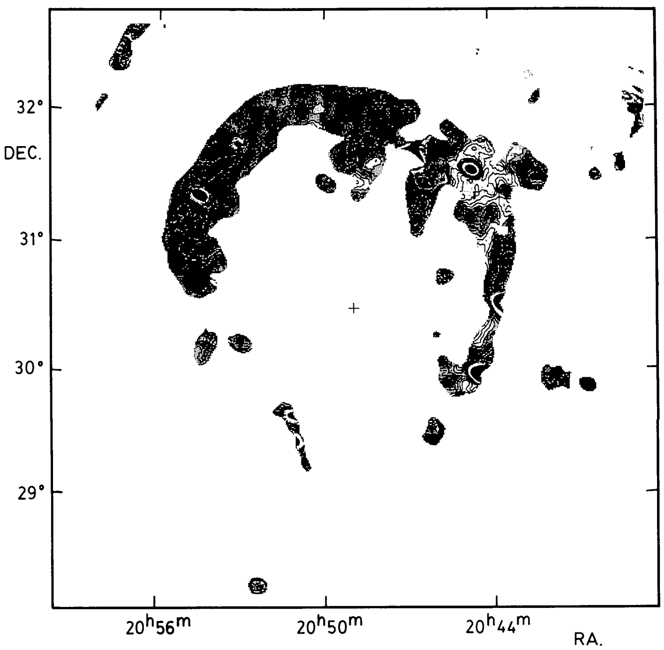

Fig. 5. The distribution of pre-shock density as determined from the ratio of the 60/100 µm images (Fig. 3c and d). The ratio was only defined where the 60 and 100 µm surface brightnesses were greater than 1.20 and 2.00 MJr/sr respectively. The grey scale is based on a histogram of map intensities, becoming darker for larger ratios. The linear contour levels are at 55–61 % in steps of 0.5 %

ignored.) Since a spatially varying contribution of recombined gas is mixed with the shock-heated component it is difficult to accurately estimate the implied density contrast. Assuming a fixed average ratio of recombined to shock-heated flux at 100 µm, ($S^R_{100}/S^S_{100} = 0.254$), the observed range in flux ratios, $S_{60}/S_{100} = 0.57$ for Balmer line filaments and $S_{60}/S_{100} = 0.60$ for the forbidden line filaments corresponds to peak wavelengths $\lambda_{peak} = 43.8$ and 42.3 µm respectively (in λI_λ) and implies a density contrast of ~ 3. This is considerably less than the factor ~ 10 expected from the range of shock velocities, but probably reflects the larger than average contribution of cool recombined gas associated with the highest density filaments. A substantial degree of beam dilution is also likely to be present which would further diminish the apparent contrast. The lowest implied densities which can be measured occur in the northwest where $S_{60}/S_{100} = 0.555$, which corresponds to $\lambda_{peak} = 44.4\ \mu m$ (using the same assumptions as above) and a density contrast of ~ 5 with respect to the forbidden line filaments. It should be noted that similar pre-shock densities are implied for the western, north-central and eastern optical filaments, supporting the assumption of similar radial and tangential velocities used in deriving the distance in Sect. 2.

The mass of high density gas which lies within the shock, assuming a time independent volume filling factor is

$$M_c = f_c \tfrac{4}{3} \pi r^3 \mu\, m_H n_c = 150\, M_\odot \quad (3)$$

(with a mean molecular weight, $\mu = 1.3$), while the kinetic energy imparted to the ISM (assuming a constant shock ram pressure and time independent mean density) is

$$E_k^{ISM} = \tfrac{1}{2} M v^2 = \tfrac{1}{2} (\tfrac{3}{4} \pi r^3 \mu\, m_H n_c)\, (\beta v_c)^2$$

$$= 0.0450 \left(\frac{r}{2\ pc}\right)^3 \left(\frac{n_c}{cm^{-3}}\right) \left(\frac{v_c}{10^3\ km\,s^{-1}}\right)^2 10^{50}\ erg$$

$$= 2.1\ 10^{50}\ erg \quad (4)$$

(cf. Braun, 1986). The implied initial SN energy driving the (~adiabatic) shock is then $E_0 = E_k^{\rm ISM}/0.283 = 7.5\ 10^{50}$ erg. This value is ~4 times greater than that found by Braun (1986) for the young SNR: Tycho, Kepler and Cas A, but in agreement with the observed trend (cf. Blair et al., 1981) for finding higher implied initial energies associated with larger diameter SNR. As Dopita (1979) quite correctly points out, in regard to this apparent relation, "no model based on an interstellar medium that is homogeneous or smoothly varying in density is consistent with the observations". This is, however, not the only indication for a systematic nonuniformity in the ISM. As discussed above, the ionization structure of the forbidden line filaments is most naturally interpreted as evidence for an abrupt radial decrease in ambient density. The observation of the X-ray plateau and non-thermal radio emission to a radius which is locally ~20 to 30% larger than the bright shell, with no associated forbidden line filaments provides further evidence that within a volume of space equal to that occupied by the bright shell no high density clouds of the type that previously gave rise to a nearly complete ring have been encountered. We are forced to conclude that the supernova which produced the Cygnus Loop occurred within a pre-existing (probably pre-cursor generated) high density bubble or shell.

The relationship between the pre-cursor's possible processing of the environment and the evolution of the ensuing SNR has recently received more consideration. McKee et al. (1984) have begun a systematic analysis of stellar wind driven bubbles in a cloudy environment which suggests that ring-like H II regions should be a common feature of O and early B star evolution in a moderate density environment just prior to leaving the main sequence. Assuming that the shell geometry is appropriate let us reconsider the mass and energy estimates above. The mass of high density gas within the shell of thickness, Δr is

$$M_c = f_c 4\pi r^2 \Delta r\, \mu\, m_H\ n_c = 35\, M_\odot \tag{5}$$

with an estimated thickness $\Delta r = 7$ arcmin $= 0.94$ pc based on the optical filament distribution (cf. Fesen et al., 1982), while the kinetic energy of shocked ISM is

$$\begin{aligned} E_k^{\rm ISM} &= \tfrac{1}{2} M v^2 = \tfrac{1}{2}(4\pi r^2 \Delta r \mu m_{\rm H} n_c)\ (\beta v_c)^2 \\ &= 0.0169 \left(\frac{r}{10\,{\rm pc}}\right)^2 \left(\frac{\Delta r}{\rm pc}\right)\left(\frac{n_c}{{\rm cm}^{-3}}\right)\left(\frac{v_c}{10^2\,{\rm km\,s}^{-1}}\right)^2 10^{50}\,{\rm erg} \\ &= 0.50\ 10^{50}\,{\rm erg} \end{aligned} \tag{6}$$

and $E_0 = 1.8\ 10^{50}$ erg. The resulting energies are fully consistent with energy estimates for young galactic SNR. Matching the energy within the shell to that of the inner sphere ($r \sim 11$ pc) before encountering the shell [Eq. (6)] allows calculation of the pressure ratio, $F = n_c v_c^2 / n_i v_i^2 = 3.3$. This is similar to the maximum pressure ratio predicted by McKee and Cowie (1975), $F = 3.15$ which is appropriate for conditions of high density contrast such as we have assumed. This provides a further indication for the consistency of our interpretation and suggests that high shock velocities $v_i > 1000$ km s^{-1} and correspondingly low densities $n_i < 0.07$ cm^{-3} were present in the interior. The interior mass would then be $M_i < 14\, M_\odot$ and the time to reach the shell, $t_i < 4400$ yr. Since systematic ionization structure is also a general phenomenon (eg. IC 443, Fesen et al., 1982; LMC SNR, Lasker, 1977) it seems likely that the explanation for the apparent E_0-diameter relation is that most shell-type forbidden line SNR are the result of pre-existing shells.

4. Conclusion

The body of observational evidence has led us to conclude that the Cygnus Loop was most probably the result of a supernova near the center of a dense pre-existing shell. The points which have led us to this conclusion are the following. 1. An X-ray plateau is observed (Ku et al., 1984) which extends to 20 to 30% larger radius than the bright filamentary shell, implying that the outer shock has progressed at least this far. Similar indications are seen in extensions of non-thermal radio emission (Green, 1984) and the emission from shock-heated dust. There is a notable absence within this external volume (as large as that of the entire filamentary shell) of high density clouds of the type which earlier gave rise to the relatively complete interior shell. 2. Narrow band optical imaging (Fesen et al., 1982) has shown a systematic radial increase of ionization state within the thick layer of optical filaments. This trend continues to the Balmer line filaments (Raymond et al., 1980) at yet larger radii. The most natural explanation of this trend is the presence of a relatively abrupt density decrease beyond the bright filamentary system, such as is also implied by point 1. above. 3. If a constant mean density is assumed to describe the pre-SNR environment, the implied initial energy is a factor ~4 larger than that found for young galactic SNR of both SNI and SNII. If the spread in initial blast wave energies is small, as seems likely, there is no plausible mechanism for producing an increase in energy with diameter in remnants not known to be associated with neutron stars. But even if there were a substantial energy spread, it is statistically improbable that it would lead to the apparent energy-diameter correlation observed. The most natural solution to this dilemma is the adoption of a pre-SNR shell geometry, for which fully consistent energy estimates result.

Although the observation discussed in point 1. above requires high sensitivity for detection in other SNR, points 2. and 3. have already been recognized as general properties of shell-type forbidden line SNR (Lasker, 1977; Dopita, 1979; Blair et al., 1981; Fesen et al., 1982). We therefore suggest that the existence of a pre-SNR shell is a common phenomenon and is in fact the reason that most evolved SNR are observable at all. Moreover, it is then the structure of the pre-cursor shell which is responsible for the morphological types found among evolved remnants. The dichotomy in optical nebulosity which distinguishes, for example, the Cygnus Loop and IC 443 from S147 and Vela (Van den Bergh et al., 1973) would then reflect the form of the wind-blown bubble(s). The frequent appearance of multiple rings with various diameters and centers (e.g. S147) in the nebulosity of a single SNR is naturally explained as the result of several pre-existing, interconnected stellar bubbles. A relatively "clean" remnant such as the Cygnus Loop implies one dominant, nearly spherical pre-SN bubble. But this suggestion may also account for large scale morphological peculiariaties such as double shells of substantially different radii (e.g. VRO 42.05.01). While it is true that by invoking a pre-existing structure to explain such morphologies one is merely transferring the problem to another domain, there is an important difference. Attempts to model the large scale incongruities of objects like VRO 42.05.01 have centered, naturally enough, on substantial (in some respects implausible) inhomogeneities in the ISM. In the case of stellar shells both the structure of the ISM and the distribution of massive stars together determine the structure of the pre-SN bubble and hence that of the remnant. Even such extreme morphological types as CTB 80 (Angerhofer et al., 1981) may be plausibly accounted for in this scenario.

Acknowledgements. RB acknowledges the financial support of the Netherlands Foundation for Astronomical Research (ASTRON) which is supported by the Netherlands Organization for the Advancement of Pure Research (Z.W.O.).

References

Angerhofer, P.E., Strom, R.G., Velusamy, T., Kundu, M.R.: 1981, *Astron. Astrophys.* **94**, 313
Blair, W.P., Kirshner, R.P., Chevalier, R.A.: 1981, *Astrophys. J.* **247**, 879
Braun, R.: 1986, *Astron. Astrophys.* (in press)
Braun, R., Strom, R.G.: 1986, *Astron. Astrophys. Suppl.* **63**, 345
Braun, R., Goss, W.M., Caswell, J.L., Roger, R.S.: 1986, *Astron. Astrophys.* (in press)
Charles, P.A., Kahn, S.M., McKee, C.F.: 1985, *Astrophys. J.* **295**, 456
Chevalier, R.A.: 1974, *Astrophys. J.* **188,** 501
Chevalier, R.A., Raymond, J.C.: 1978, *Astrophys. J. Letters* **225**, 127
Cowie, L.L., McKee, C.F.: 1977, *Astrophys. J.* **211**, 135
DeNoyer, L.K.: 1975, *Astrophys. J.* **196**, 479
Dickel, J.R., Willis, A.G.: 1980, *Astron. Astrophys.* **85**, 55
Dopita, M.A.: 1979, *Astrophys. J. Suppl.* **40**, 455
Draine, B.T.: 1981, *Astrophys. J.* **245**, 880
Draine, B.T.: 1985, *Astrophys. J. Suppl.* **57**, 587
Draine, B.T., Lee, H.M.: 1984, *Astrophys. J.* **285**, 84
Draine, B.T., Anderson, N.: 1985, *Astrophys. J.* **292**, 494
Fesen, R.A., Blair, W.P., Kirshner, R.P.: 1982, *Astrophys. J.* **262**, 171
Green, D.A.: 1984, *Monthly Notices Roy. Astron. Soc.* **211**, 433
Hubble, E.P.: 1937, Carnegie Inst. Yearbook 36, 189
IRAS Explanatory Supplement: 1985, eds. C.A. Beichman, G. Neugebauer, H.J Habing, P.E. Clegg, T.J. Chester
Keen, N.J., Wilson, W.E., Haslam, C.G.T., Graham, D.A., Thomasson, P.: 1973, *Astron. Astrophys.* **28**, 197
Ku, W.H.-M., Kahn, S.M., Pisarski, R., Long, K.S.: 1984, *Astrophys. J.* **278**, 615
Lasker, B.M.: 1977, *Publ. Astron. Soc. Pacific* **84**, 474
McKee, C.F., Cowie, L.L.: 1975, *Astrophys. J.* **195**, 715
McKee, C.F., Cowie, L.L., Ostriker, J.P.: 1978, *Astrophys. J.* **219**, L23
McKee, C.F., Van Buren, D., Lazareff, B.: 1984, *Astrophys. J.* **278**, L115
Miller, J.S.: 1974, *Astrophys. J.* **189**, 239
Minkowski, R.: 1958, *Rev. Mod. Phys.* **30**, 1048
Raymond, J.C.: 1979, *Astrophys. J. Suppl.* **39**, 1
Raymond, J.C., Davis, M., Gull, T.R., Parker, R.A.R.: 1980, *Astrophys. J.* **238**, L21
Raymond, J.C., Blair, W.P., Fesen, R.A., Gull, T.R.: 1983, *Astrophys. J.* **275**, 636
Scoville, N.Z., Irvine, W.M., Wannier, P.G., Predmore, C.R.: 1977, *Astrophys. J.* **216**, 320
van den Bergh, S., Marscher, A.P., Terzian, Y.: 1973, *Astrophys. J. Suppl.* **26**, 19